Frustrated magnetic vortices in hexagonal lattice of magnetic nanocaps

M. V. Sapozhnikov,[1] O. L. Ermolaeva,[1] B. G. Gribkov,[1] I. M. Nefedov,[1] I. R. Karetnikova,[1] S. A. Gusev,[1] V. V. Rogov,[1] B. B. Troitskii,[2] and L. V. Khokhlova[2]

[1]*Institute for Physics of Microstructures RAS, 603950, Nizhny Novgorod GSP-105, Russia*

[2]*G. A. Razuvaev Institute of Organometallic Chemistry Russian Academy of Sciences, Nizhny Novgorod GSP-445, Russia*

(Received 13 September 2011; revised manuscript received 23 December 2011; published 1 February 2012)

Magnetic properties of hexagonal lattices of touching magnetic nanocaps fabricated by Co film deposition on a surface of polymethyl methacrylate colloidal crystals was studied as a function of both period (120–450 nm) and thickness (30–60 nm). Magnetization configurations and hysteresis loops of the samples were investigated by magneto-optic Kerr effect and magnetic force microscopy. Formation of frustrated hexagonal lattices of magnetic vortices was found in the system. Magnetic coupling of the nanocaps can be tuned by changing the thickness of the deposited magnetic film, leading to change of the magnetization loop. Micromagnetic simulations of hexagonal lattices of touching magnetic dots complement the experimental observations corroborating the influence of the lattice period and the intercap coupling on the possible magnetization configurations in the system.

DOI: 10.1103/PhysRevB.85.054402 PACS number(s): 75.75.−c, 75.70.Kw, 75.40.Mg

I. INTRODUCTION

Recently, arrays of magnetic particles have been investigated intensely, owing to fundamental physics problems[1] and the potential applications as plasmonic material[2,3] or high-density recording media.[4,5] Particular attention has been given to the magnetic and magneto-optical properties of periodic arrays of micron and submicron elements of very different shapes,[6,7] especially dots[8–10] and stripes.[11–13] Magnetostatic interaction in the arrays of the densely packed particles has been thoroughly studied also,[14–16] as it affects the magnetic states and magnetization reversal in the system. The usual methods to fabricate nanostructured magnetic materials are different top-down lithographic techniques.[17] However, such methods are slow and cost ineffective for mass production. On the other hand, a bottom-up self-assembly method such as metal deposition on the surface of colloidal crystal[18] makes it possible to fabricate regular two-dimensional (2D) lattices of magnetic nanocaps.[19] The specific feature of such lattices is direct exchange coupling between neighboring nanocaps. The effects of the intercap interaction on magnetization reversal of arrays of the magnetically coupled Co/Pd and Gd/Fe nanocaps with out-of-plane anisotropy[20–23] and magnetoresistive effects in them[24] have been studied recently.

In this work we investigate a magnetization reversal and magnetic states of 2D hexagonal lattice of closely packed Co nanocaps fabricated by Co film deposition on a top of polymethyl methacrylate (PMMA) colloidal crystal. The system has in-plane anisotropy, so a lattice of magnetic vortices can be formed in the system. Due to a hexagonal symmetry of the vortex lattice the magnetic coupling will result in geometrical frustration. The similar frustration has been found in triads of permalloy rings.[25]

Why would it be interesting to investigate its magnetic properties of the studied systems? A fascinating feature of magnetic nanosystems with a geometrical frustration is a possibility to create and study artificial "spin ice" in which the individual element can be probed.[1] Most of the systems under study are lithographically manufactured arrays with magnetostatic interaction between particles.[26–28] The distinctive feature of our system is that it is frustrated due to an exchange coupling which can be easily tuned by varying the thickness of the deposited magnetic film. Besides it is known that a magnetic vortex is a state with a noncomplanar distribution of the magnetization and can demonstrate unusual electron-transport properties such as the topological Hall effect.[6,29,30] Evidently, lattice of the contacting ferromagnetic hemispheres is more suitable to carry out transport measurements than the separate nanoparticle. In our work we determine the parameters of the system when the lattice of the vortices is formed. So we think that the hexagonal lattice of magnetic nanocaps is a very promising material for future transport measurements.

II. SAMPLE PREPARATION AND EXPERIMENTAL DETAILS

PMMA particles were synthesized by polymerization of 20% MMA monomer in water solution (pH = 7.0–8.0) in the presence of potassium peroxodisulfate (0.08 wt. %) at a temperature of 80 °C under Ar atmosphere.[31] The polymerization solution was stirred at 500–600 rpm for 3–5 h. Treating the reaction mixture with air for at least 5 min stops the polymerization. The method makes it possible to synthesize the monodisperse PMMA particles with diameters 100–500 nm depending on the polymerization time. Preparation of colloidal crystals is based on self-assembly of the obtained PMMA globules suspended in an aqueous environment. Three-dimensional colloidal crystals were obtained by means of drying the suspension on a flat hydrophobized glass substrate in a closed chamber at room temperature under a pressure of 20 Torr. Thus, the colloidal crystal films with the thickness of 100–300 μm were obtained.

Ordered ferromagnetic nanostructures were prepared by magnetron sputtering of a thin Co layer on a surface of the PMMA colloidal crystal. Ar pressure during the deposition was 4×10^{-3} Torr. The growth rate for Co was 1 nm/s. To prevent oxidation, the Co layer was covered with a 2-nm-thick Si layer. So the PMMA nanospheres were hemispherically covered with the metal and the resulting film consisted of the hexagonally close-packed array of the ferromagnetic hemispheres. The period of the fabricated array is dictated by

 ©2012 American Physical Society

the template. A series of the samples with periods of 120–450 nm and thicknesses of 30 and 60 nm was manufactured. The thicknesses of the obtained Co nanocorrugated films were measured as the thickness of the reference flat Co films deposited on a glass substrate in the same run. The actual average thickness of the obtained Co nanocorrugated film is twice smaller because the ratio of the surface area of hemisphere to the surface area of its supporting circle is equal to 2 and may be nonuniform.

The morphology of the nanocorrugated films was studied by scanning electron microscopy (SEM) and by atomic-force microscopy (AFM, "Solver-HV," NT-MDT). The field emission scanning electron microscope with a Schottky Field emissions gun was used during this investigation. The topography of uncoated PMMA colloidal crystals was studied in low-voltage mode (energy of primary electron beam is 1 to 2.5 kV) or in low-vacuum mode with SEM Supra 50VP (Carl Zeiss). The investigations show that the size of the colloidal crystal crystallites with different orientations of the crystal axes is 30–50 μm. The specimens coated by Co films were studied with a Neon 40 CrossBeam station (Carl Zeiss), equipped with a focused ion beam (FIB) system (minimal ion beam diameter is about 7 nm). For observing secondary electron (SE) images of the specimens both the in-lens and the Everhardt Thornley detectors were used. The optimum SE imaging conditions were attained with the incident-electron energy set at 10 kV with the e-beam current 0.3 nA, which produced images with resolution on the order of 3 nm. The FIB was used to cut individual PMMA particles for the visualization of material contrast between PMMA and Co on cross sections with backscattered electrons (resolution of images is about 5 nm).

A magneto-optical Kerr effect (MOKE) for the samples was measured with a home-built system in meridional configuration. A linearly polarized He-Ne ($\lambda = 632$ nm, 5 mW power) laser was used as a light source. The laser light was further polarized by a Glan-Thompson polarizer and was incident on the sample surface at 40° off the normal. The reflected beam passed through a Faraday modulator providing a polarization modulation at frequency 400 Hz. After passing a second Glan-Thompson polarizer, the reflected light was detected by a photodiode. The photodiode signal was measured with a lock-in amplifier. The samples were mounted inside a gap of an electromagnet which allowed magnetic fields of up to 3 KOe to be applied in the plane of the sample. During the measurement, data were taken as a function of magnetic field to generate a hysteresis loop.

The magnetic states of the Co hemispheres were studied using a vacuum scanning probe magnetic force microscope "Solver-HV," which was equipped with a dc electromagnet incorporated in a vacuum vibration insulating platform. The scanning probes were Co coated with a thickness of 30 nm. The tips were magnetized along the symmetry axes in a 10 kOe external magnetic field before the measurements. The magnetic force microscopy (MFM) measurements were performed in a noncontact constant-height mode. A phase shift of cantilever oscillations under the gradient of the magnetic field of a sample was registered to obtain the MFM contrast. All measurements were performed in a vacuum of 10^{-4} Torr, which improved the MFM signal due to an increase in the cantilever quality factor.

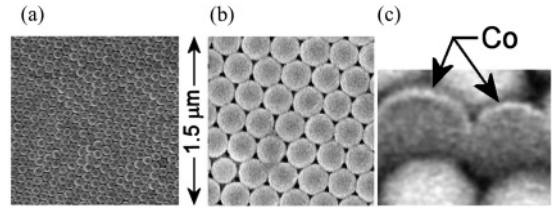

FIG. 1. (a),(b) SE images of the 30 nm Co film on the top of the colloidal crystals with the period 120 and 370 nm correspondingly. (c) Microphotography of the particles cross-section made by focused Ga^+ ion beam. The image observed with backscattered electrons ($E = 3$ kV), the Co coverage is visible as bright layer.

III. EXPERIMENTAL RESULTS AND DISCUSSION

In-plane MOKE hysteresis loops of the samples are summarized in Fig. 2. Three classes of the loops were observed. The first type [Fig. 2(a)] is typical for arrays of nanocaps with diameters larger than 250 nm and a thickness of 30 nm. The 8-like shape of the hysteresis loops with zero remanent magnetization indicates that the magnetization has a vortex distribution[8] in the nanocaps. In this case, the magnetization process takes place by pushing the vortex core away from the center of a nanocap. At some critical field (several hundreds of Oe) the vortex becomes unstable and leaves a nanocap. When the magnetic field is decreased from the saturation, a magnetic vortex nucleates, accompanied by an abrupt decrease in magnetization. MFM observations confirm the vortex structure in remanence for the samples, as well as single-domain-like

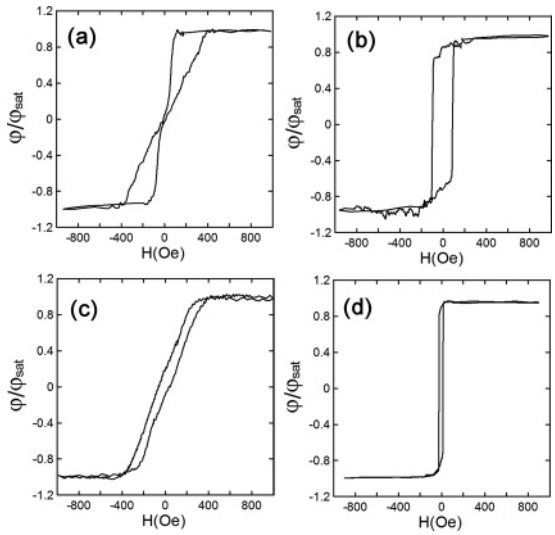

FIG. 2. In-plane magnetization curves of the lattices of the Co nanocaps measured by the magnetooptic Kerr rotation. (a) Hysteresis loop of the 30-nm Co film deposited on the top of the PMMA colloidal crystal (the particle diameter is 340 nm). The loop corresponds to the vortex distribution of the magnetization in the caps. (b) Hysteresis loop of the 30-nm film deposited on the top of the PMMA colloidal crystal (the particle diameter is 120 nm). The loop corresponds to the single-domain distribution of the magnetization in caps. (c) Hysteresis loop of the 60-nm film deposited on the top of PMMA colloidal crystal (particle diameter 290 nm). The loop corresponds to the mixed states of the magnetization distribution in the system. (d) Hysteresis loop of the flat control Co film.

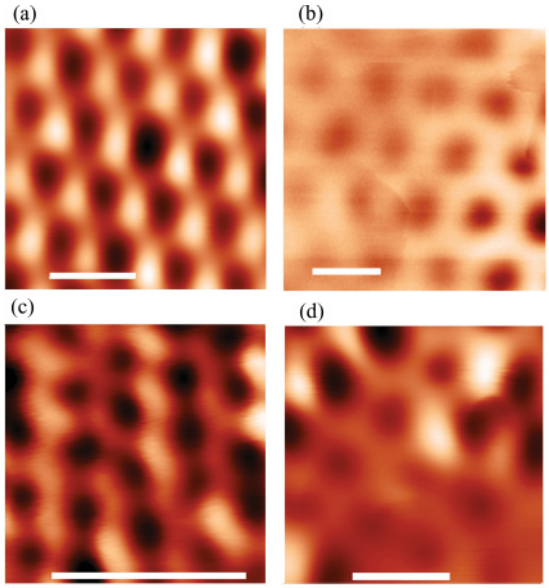

FIG. 3. (Color online) Experimental MFM images of the lattices of the Co nanocaps in different magnetic states at zero magnetic field. The length of the scale bar is equal to 400 nm. (a) MFM image of the lattice of the Co nanocaps (the particle diameter is 290 nm; Co thickness is 30 nm) at 200 Oe after magnetizing to the saturation at 1000 Oe. (b) The lattice of the magnetic vortices. (c) The lattice of single-domain states magnetized uniformly in the remanent state at zero magnetic field (the particle diameter is 120 nm; Co thickness is 30 nm). (d) The mixed distribution of the magnetization; both vortices and single-domain states are visible (the particle diameter is 290 nm; Co thickness is 60 nm). The particles with single-domain distribution produces two magnetic poles; the particles within vortex state produces less signal with centrally symmetric contrast.

state in the saturation. Experimental MFM images of these states are shown in Figs. 3(a) and 3(b). At saturation when the particles are in the single-domain states the bright and dark poles are visible [Fig. 3(a)]. At zero external field the picture is quite different. In this case we observed centrally symmetric contrast distribution of the MFM signal of each particle, and the signal amplitude becomes significantly less. It is due to the fact that magnetic vortices do not cause leakage magnetic fields with the exception of the weak vortex core leakage field. The signal of cores is weak and can be observed in the case of flat particles on the conducting substrate.[32,33] Our samples have very uneven surface due to nanocorrugation and the substrate is dielectric. So the observed field in the case of the vortices is primarily due to electrostatic interaction of the MFM tip with the surface; unfortunately, it is impossible to observe cores in such conditions.

A second class of the hysteresis loops is typical for the arrays of nanocaps with diameters less than 250 nm and a thickness of 30 nm [Fig. 2(b)]. These loops have a rectangular shape and retain a high remanence and the switching field is about 100–150 Oe. The shape of the loops is usual for the particles in single-domain states, which is confirmed by MFM investigation [Fig. 3(c)]. In this case the magnetization reversal occurs by simultaneous abrupt reversal of all ferromagnetic hemispheres. The control flat Co film obtained in the same deposition process does not have in-plane anisotropy axes

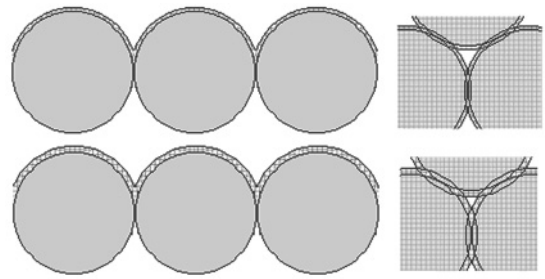

FIG. 4. Top and cross-section side schematic views of a Co layer coating the PMMA colloidal crystal surface for different coating thicknesses. The thicker coating caused larger overlapping.

and its coercivity is equal to 20 Oe [Fig. 3(d)]. The increase of the coercivity of the nanostructured film up to 100 Oe is due to geometrical anisotropy of the ordered structure of the nanocaps.

The transition from the vortex to single-domain distribution of the magnetization was observed in the system with the decrease of the nanocap radius. Such transition is well known for the nanomagnets of the circular shape.[8] The situation becomes quite different in our case for the samples with thicker Co nanocaps. With the increase of the Co coverage up to 60 nm magnetization loops obtain parallelepiped shape with a significant side slope [Fig. 2(c)]. The system has a small nonzero remanent magnetization in this case. MFM measurements showed that at zero external field the magnetization distribution in the array is a mixture of the vortex and single-domain states [Fig. 3(d)]. In the case of the large-enough nanocaps (with the diameter 450 nm) they keep the vortex magnetization distribution and the corresponding hysteresis loop shape even in the case of the 60-nm Co coverage.

In order to interpret such behavior we should take into account that the increase of the metal film thickness leads to an increase of the overlapping of the contacting nanocaps (Fig. 4). While in the case of the thin Co coverage ferromagnetic caps on top of PMMA spheres are nearly isolated, in the case of the thicker coverage the overlap significantly increases. This leads to an increase of the role of an exchange interaction between the nanocaps.

In the case of two contacting nanocaps with the vortex distribution of the magnetization within them, two configurations are possible. If the vortices have different signs of vorticity, their magnetizations in the contact point will be parallel and the energy of the system will be decreased due to negative contribution of the exchange energy. On the contrary, two contacting vortices with the same vorticity have the antiparallel orientation of the magnetizations in the contact point, which will increase the energy of the system. In the case of the square lattice the vortices with the different vorticity will be staggered to reduce the exchange energy in the every contact point, but this is impossible in the case of the hexagonal lattice. The system of the vortices on the hexagonal lattice will be frustrated and at least 1/3 of the contact points will have antiparallel directed magnetizations. So the energy of the frustrated lattice of the vortices increases as the Co coverage becomes thicker. The system releases this frustration by transition of the same nanocaps in the single-domain state. Such a mixed state is observed at the zero external field.

IV. MICROMAGNETIC MODELING

In order to better understand the influence of the exchange interaction between magnetic nanocaps on the magnetization distribution in the system we performed micromagnetic simulations. Actually, we cannot numerically simulate the problem of 3D magnetization distribution in the array of significantly large (up to 450 nm) interacting nanocaps. Therefore, we numerically simulated topologically similar but easier 2D problem of a magnetization distribution in hexagonal arrays of contacting flat magnetic dots. The increase of a hemisphere thickness corresponds to the increase of the supporting circle diameter (Fig. 4). So the change of the hemisphere thickness is mimicked by the changing of the nanodot diameters in the 2D simulations. To overlap the dots their diameters were slightly larger than the lattice period. Evidently, the magnetic vortices will be frustrated in the same way in the both system.

The model system for the calculations was a cell of the hexagonal lattice which contains 16 particles with the periodic boundary conditions [Fig. 5(d)]. We study the lattices with the periods from 100 to 400 nm. The thicknesses of the particles were 15 and 30 nm in our calculations. As mentioned above, this corresponds to the actual thickness of the experimentally investigated hemispheres. The simulation was performed using SIMMAG special program package[34] based on a numerical solution of the Landau-Lifshitz-Gilbert (LLG) system of equations for the magnetization of the system:

$$\frac{\partial \vec{M}}{\partial t} = -\gamma(\vec{M} \times \vec{H}_{\text{eff}}) - \frac{\gamma d}{M_s}[\vec{M} \times (\vec{M} \times \vec{H}_{\text{eff}})], \qquad (1)$$

where M is the magnetization, γ is the gyromagnetic ratio, d is the dimensionless damping parameter, and M_s is the magnetization at saturation. The effective field $\vec{H}_{\text{eff}} = -\delta E/\delta \vec{M}$ is a variation derivative of the energy function. The total energy of the particle can be defined by

$$E = E_h + E_{\text{ex}} + E_m. \qquad (2)$$

The first term E_h is the energy of the interaction between the particle magnetization and an external magnetic field H. The second term E_{ex} is the energy of the exchange interaction and E_m is the demagnetization energy of the dot. Expressions for these terms have conventional form.[35,36] All calculations were carried out for parameters of cobalt $J = 3 \times 10^{-6}$ erg/cm, $M_s = 1400$ emu/cm^3, and damping constant $d = 0.5$. While the anisotropy of the epitaxial Co film or bulk material is high enough [anisotropy constant $K_1 = 6.5 \times 10^5$ erg/cm^{-3})], in the case of the polycrystalline Co films average magnetocrystalline anisotropy is very small and it was shown that anisotropy term can be neglected in magnetization distribution simulations.[37] Because (1) the primary aim of our simulations is the understanding of the interplay between the magnetostatic and exchange energy in the hexagonal lattice of the contacting ferromagnetic nanoparticles and (2) actually experimentally measured coercivity is small and anisotropy is absent in the flat control Co films, we omitted the magnetic anisotropy term in Eq. (2), assuming polycrystalline structure of the particles.

The model distributions were obtained as the stationary solutions of the system of the LLG equations for the magnetization on a square grid. The grid cell size was selected to be from 5 nm for the lattices with the 400-nm period to 2 nm for the lattices with 100-nm period. We calculated the energy of the system with the dots in the single-domain states oriented in the same direction and for the system with the dots in vortex states. There are 48 contact points between the 16 dots within the chosen lattice cell. Depending on the number of the clockwise and anticlockwise vortices and their distribution through the lattice there will be from 1 to 3 contact points with antiparallel configuration of the magnetization per dot. Evidently, total interdot exchange energy will be proportional to the average number of contacts with antiparallel configuration. We calculated the minimum and maximum possible energies of the frustrated vortex lattice. In the first case the vortices was distributed in the system as it is shown on the Fig. 5(b), in the second case all vortices had the same direction of the vorticity. The calculations were done in the following way. We started from the proper initial conditions which were the uniformly magnetized system or the system with the studied vortex distributions and let the magnetization distribution relax to the local energy minimum. The typical results of the energy calculations are represented in Fig. 6 for the system with the period of 300 nm. The energy of the lattice

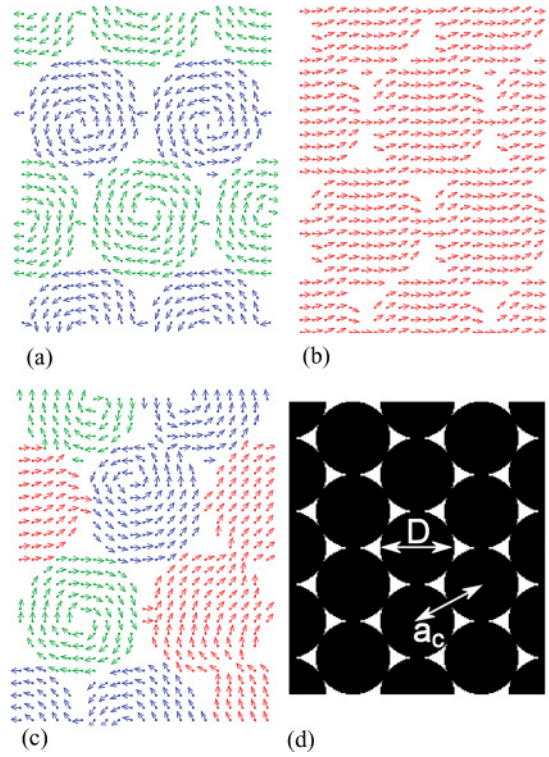

FIG. 5. (Color online) The possible magnetization configurations numerically simulated on hexagonal lattices of overlapping magnetic nanodots. A part of the simulated lattice is shown. The lattice constant is 300 nm; dot diameter is 303 nm. Arrows represent the magnetization of 5 × 5-nm cell of the computational grid, only 1/36 of arrows are shown. (a), (b), and (c) are vortex (the case with the minimal energy when only 1/3 of the interdot contacts are antiferromagnetically aligned), single-domain, and mixed distributions of the magnetization. Clockwise and anticlockwise vortices are denoted by green and blue colors, respectively; single-domain states are denoted by red color. (d) Unit cell of the simulated system. a_c is the period of the lattice of the magnetic dots; D is their diameter. $D > a_c$ to overlap the dots.

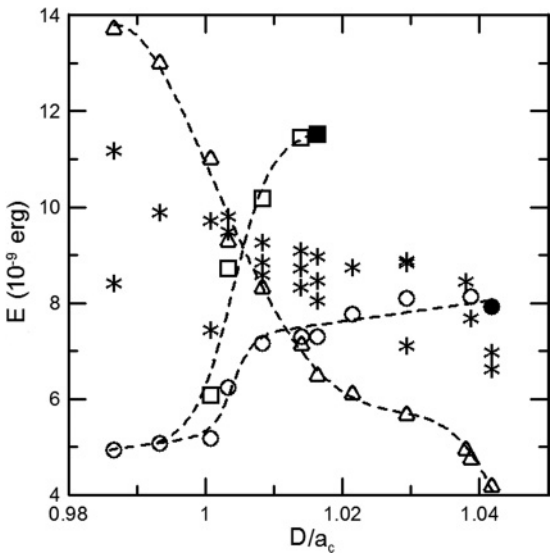

FIG. 6. Calculated energies of the magnetic configurations for different ratios between magnetic disk diameter (D) and lattice constant ($a_c = 300$ nm). Triangles denote the energy of the system with the dots in the single-domain states. Squares denote the energies of the frustrated lattices of the magnetic vortices for the configuration when all interdot contacts are antiferromagnetically aligned. The circles are for the lattice of the magnetic vortices configuration when 1/3 of the interdot contacts are antiferromagnetically aligned while 2/3 are aligned ferromagnetically. The solid square and the solid circle are for the maximum D/a_c value when the corresponding vortex configurations remain stable. Stars denote the energies of different mixed configurations. The dashed lines are guides for the eyes.

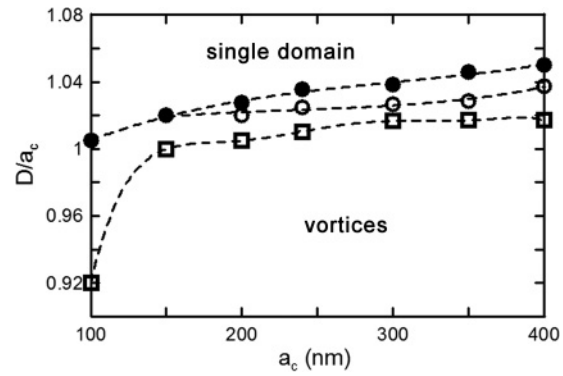

FIG. 7. Phase diagram of the magnetic states of the hexagonal lattice of the Co nanocaps. a_c is the lattice period, D is the magnetic dot diameter.Squares corresponds to the parameters when the the energies of the lattice of the magnetic vortices (with 1/3 of antiferromagnetically aligned interdot contacts) and uniformly magnetized single-domain states are equal. The open circles is for the parameters of the system the vortices begin to shifts from the central position. The solid circles is corresponds to the parameters values when the vortex lattice becomes unstable. The dashed lines are guides for eyes.

of the single-domain dots gradually decreases as the size of the dots increases. It is due to the decrease of the interparticle voids accompanied by decrease of the demagnetizing energy.

The dependence of the energy of the vortex lattice on the particle size has two plateaus divided by the region of the energy growth. This growth of the energy begins when the particles come to contact. With the increase of the overlapping of the dots the exchange energy increases due to the contacts with antiparallel directions of magnetization. With the further increase of the particle overlapping two scenarios are possible. In the case of the smaller lattice periods the vortices become unstable and the system passes to the state with the single-domain distribution of the magnetization within the particles. For the larger periods the second plateau is observed. In this case there is still vortex distribution of the magnetization within the particles, but the vortex cores are shifted from the central positions.

Evidently there are a number of possible mixed states [Fig. 5(c)] with various magnetization configurations which have different energy values. In Fig. 6 the energies of the several possible mixed states obtained by numerical simulations are represented. We used the following procedure for the simulations. Starting with random distribution of the magnetization we let the system relax to the nearest energy minimum. So we calculated the energies of a number of different mixed states. It turned out that if dots do not make contact or interdot contacts are small in size the energy of the vortex lattice is smaller than the energy of the mixed states, so the magnetization reversal between the uniformly magnetized states takes place through the creation of the vortex states within the dots. With the increase of the dots overlapping the energy of some mixed states becomes less than the energy of the frustrated vortex lattice. In this case the magnetization reversal, which is observed in the experiment, takes place through the formation of the sequence of mixed states producing the magnetization curve slope [Fig. 2(c)].

The summary of the configuration energies is represented in Fig. 6. The energy of the single-domain state decreases while the energy of the vortex state increases with the interdot overlapping increase. So they become equal at some point. The position of this point depends on the lattice period (Fig. 7). With the increase of the period of the structure the vortices become more stable and the larger overlapping of the particles is possible before the vortices become unstable. The change of the dot thickness from 15 to 30 nm without changing their diameters slightly increases the stability of the vortices as well, as is known for the separate dots.[8,38]

V. SUMMARY

The hexagonal lattices of contacted magnetic nanocaps exhibit a magnetic reversal process that is strongly affected by the intercap exchange interacting as measured by MOKE. At remanence, the system yields the vortex magnetization configuration in nanocaps. However, the formation of vortices on a hexagonal lattice is frustrated due to an exchange interaction between the Co nanocaps. The increase of the Co layer thickness leads to an increase in the nanocaps overlapping and so to an increase of the exchange interaction between them. The latter results in the formation of the mixed state (both the single-domain and vortex states are present) after demagnetizing the system from saturation. The decrease in the particle size accompanied with a decrease of magnetostatic energy of the system and results in the

single-domain states of the nanocaps. This magnetization states were experimentally verified by MFM. We also reported here the results of micromagnetic modeling of magnetic states in a hexagonal lattice of overlapping magnetic dots with an exchange interaction. In spite of the difference in the shape of the disk and nanocap the model system demonstrates all experimentally observed states.

ACKNOWLEDGMENTS

We are grateful to A. Yu. Aladyshkin for fruitful discussions. This research was supported by RFBR, the RF Agency for Education of Russian Federation (Rosobrazovanie), and the Agency for Science and Innovation of the Russian Federation.

[1] R. F. Wang, C. Nisoli, R. S. Freitas, J. Li, W. McConville, B. J. Cooley, M. S. Lund, N. Samarth, C. Leighton, V. H. Crespi, and P. Schiffer, Nature (London) **439**, 303 (2006).
[2] Z. Liu, L. Shi, Z. Shi, X. H. Liu, J. Zi, S. M. Zhou, S. J. Wei, J. Li, X. Zhang, Y. J. Xia, Appl. Phys. Lett. **95**, 032502 (2009).
[3] M. V. Sapozhnikov, S. A. Gusev, B. B. Troitskii, and L. V. Khokhlova, Opt. Lett. **36**, 4197 (2011).
[4] S. D. Bader, Rev. Mod. Phys. **78**, 1 (2006).
[5] C. L. Chien, F. Q. Zhu, and J.-G. Zhu, Phys. Today **60**, 40 (2007).
[6] V. L. Mironov, O. L. Ermolaeva, S. A. Gusev, A. Yu. Klimov, V. V. Rogov, B. A. Gribkov, O. G. Udalov, A. A. Fraerman, R. Marsh, C. Checkley, R. Shaikhaidarov, and V. T. Petrashov, Phys. Rev. B **81**, 094436 (2010).
[7] S. P. Li, D. Peyrade, M. Natali, A. Lebib, Y. Chen, U. Ebels, L. D. Buda, and K. Ounadjela, Phys. Rev. Lett. **86**, 1102 (2001).
[8] R. P. Cowburn, D. K. Koltsov, A. O. Adeyeye, M. E. Welland, and D. M. Tricker, Phys. Rev. Lett. **83**, 1042 (1999).
[9] J. Raabe, R. Pulwey, R. Sattler, T. Schweinbock, J. Zweck, and D. Weissa, J. Appl. Phys. **88**, 4437 (2000).
[10] M. Schneider, H. Hoffmann, and J. Zweck, Appl. Phys. Lett. **77**, 2909 (2000).
[11] A. O. Adeyeye, G. Lauhoff, J. A. C. Bland, C. Daboo, D. G. Hasko, and H. Ahmed, Appl. Phys. Lett. **70**, 1046 (1997).
[12] M. Pratzer and H. J. Elmers, Phys. Rev. B **66**, 033402 (2002).
[13] X. Kou, X. Fan, R. K. Dumas, Q. Lu, Y. Zhang, H. Zhu, X. Zhang, K. Liu, and J. Q. Xiao, Adv. Mater. **23**, 1393 (2011).
[14] A. A. Fraerman, S. A. Gusev, L. A. Mazo, I. M. Nefedov, Yu. N. Nozdrin, I. R. Karetnikova, M. V. Sapozhnikov, I. A. Shereshevskii, and L. V. Sukhodoev, Phys. Rev. B **65**, 064424 (2002).
[15] J. L. Costa-Kramer, R. Alvarez-Sanchez, A. Bengoechea, F. Torres, P. Garcia-Mochales, and F. Briones, Phys. Rev. B **71**, 104420 (2005).
[16] A. Remhof, A. Schumann, A. Westphalen, H. Zabel, N. Mikuszeit, E. Y. Vedmedenko, T. Last, and U. Kunze, Phys. Rev. B **77**, 134409 (2008)
[17] J. I. Martin, J. Nogues, K. Liu, J. L. Vicent, and I. K. Schuller, J. Magn. Magn. Mater. **256**, 449 (2003).
[18] J. Q. Liu, A. I. Maaroof, L. Wieczorek, and M. B. Cortie, Adv. Mater. **17**, 1276 (2005).
[19] M. Albrecht, G. Hu, I. L. Guhr, T. C. Ulbrich, J. Boneberg, P. Leiderer, and G. Schatz, Nat. Mater. **4**, 203 (2005).
[20] T. C. Ulbrich, C. Bran, D. Makarov, O. Hellwig, J. D. Risner-Jamtgaard, D. Yaney, H. Rohrmann, V. Neu, and M. Albrecht, Phys. Rev. B **81**, 054421 (2010).
[21] C. M. Gunther, O. Hellwig, A. Menzel, B. Pfau, F. Radu, D. Makarov, M. Albrecht, A. Goncharov, T. Schrefl, W. F. Schlotter, R. Rick, J. Luning, and S. Eisebitt, Phys. Rev. B **81**, 064411 (2010).
[22] E. Amaladass, B. Ludescher, G. Schutz, T. Tyliszczak, M.-S. Lee, and T. Eimuller, J. Appl. Phys. **107**, 053911 (2010).
[23] N. Mikuszeit, L. Baraban, E. Y. Vedmedenko, A. Erbe, P. Leiderer, and R. Wiesendanger, Phys. Rev. B **80**, 014402 (2009).
[24] J. K. nee Moser, V. Kunej, H.-F. Pernau, E. Scheer, and M. Albrecht, J. Appl. Phys. **107**, 09C506 (2010).
[25] V. Rose, K. Buchanan, S.-H. Chung, M. Grimsditch, V. Metlushko, A. Hoffmann, V. Novosad, S. D. Bader, and H. Ibach, Phys. Rev. B **73**, 094442 (2006).
[26] Y. Qi, T. Brintlinger, and John Cumings, Phys. Rev. B **77**, 094418 (2008).
[27] G. Moller and R. Moessner, Phys. Rev. Lett. **96**, 237202 (2006).
[28] X. Ke, J. Li, C. Nisoli, P. E. Lammert, W. McConville, R. F. Wang, V. H. Crespi, and P. Schiffer, Phys. Rev. Lett. **101**, 037205 (2008).
[29] A. Neubauer, C. Pfleiderer, B. Binz, A. Rosch, R. Ritz, P. G. Niklowitz, and P. Boni, Phys. Rev. Lett. **102**, 186602 (2009).
[30] P. Bruno, V. K. Dugaev, and M. Taillefumier, Phys. Rev. Lett. **93**, 096806 (2004).
[31] B. B. Troitskii, L. V. Khokhlova, V. N. Denisova, M. A. Novikova, D. A. Smirnov, and M. A. Baten'kin, Russ. J. Appl. Chem. **80**, 1424 (2007).
[32] M. Natali, I. L. Prejbeanu, A. Lebib, L. D. Buda, K. Ounadjela, and Y. Chen, Phys. Rev. Lett. **88**, 157203 (2002).
[33] H. Shima, V. Novosad, Y. Otani, K. Fukamichi, N. Kikuchi, O. Kitakamai, and Y. Shimada, J. Appl. Phys. **92**, 1473 (2002).
[34] The program was developed in the Institute for Physics of Microstructures of the Russian Academy of Sciences; I. M. Nefedov, I. R. Karetnikova, I. A. Shereshevskii, *XII International Symposium "Nanophysics and nanoelectronics,"* Vol. 2, p. 277, (Institute of Microstructures RAS, Nizhny Novgorod, Russia, 2008).
[35] E. D. Boerner and H. N. Bertran, IEEE Trans. Magn. **33**, 3052 (1997).
[36] A. A. Fraerman, I. M. Nefedov, I. R. Karetnikova, M. V. Sapozhnikov, and I. A. Shereshevskii, Phys. Met. Metallogr. **92** (supplementary issue 1), 226 (2001).
[37] M. Klaui, C. A. F. Vaz, L. Lopez-Diaz, and J. A. C. Bland, J. Phys. Condens. Matter **15**, R985 (2003).
[38] I. L. Prejbeanu, M. Natali, L. D. Buda, U. Ebels, A. Lebib, Y. Chen, and K. Ounadjela, J. Appl. Phys. **91**, 7343 (2002).